Progress In Electromagnetics Research, PIER 87, 15–41, 2008

MANEUVERING TARGET DOPPLER-BEARING TRACKING WITH SIGNAL TIME DELAY USING INTERACTING MULTIPLE MODEL ALGORITHMS

S. Z. Bi and X. Y. Ren

Department of Information and Electronic Engineering
Zhejiang University
Hangzhou 310027, China

Abstract—For maneuvering target Doppler-bearing tracking with signal time delay, a novel approach called ISE-IMM is proposed in this paper. The iterative state estimation (ISE) method is designed to eliminate the negative influence of time delay effect and an interacting multiple model (IMM) filter is embedded to estimate the state according to the measurements of the delayed signal. The nonlinear filter preferred in this paper is a particle filter (PF) with an improved resampling procedure. Performance of our proposed method is evaluated in Monte Carlo simulations. Results show the effectiveness and stability of ISE-IMM-PF in combating the negative effect of signal time delay.

1. INTRODUCTION

Recent studies have applied multifarious new techniques to radar systems [1–9]. Radar systems detect the position and velocity of a target based on received measurements. Among various radar systems, passive radar system has advantages such as lower costs of operation and maintenance, better resilience to anti-radiation technology, etc. In passive tracking problems, the target trajectory is estimated based on the measurements of signals emitted by the target. The most common target motion analysis (TMA) tracks the kinematics of the target using noise-corrupted bearing measurements and it is well known as bearing-only tracking (BOT). When the tonal signal is narrow banded, frequency measurement is also available [10]. Since the received signal frequency is Doppler shifted, the TMA problem with both bearing and frequency measurements is sometimes referred to as Doppler-bearing tracking (DBT).

Algorithms to solve BOT problem are well investigated in the last decade [11–13], nevertheless DBT has its inherent advantages over BOT [14]: the additional frequency measurements provide extra target course and speed information, making DBT more observable than BOT [14]. The conditions are that the emitted frequency must be constant during observation time and the target is not moving radially. In such situations, the observer can be stationary [15], which is very useful in real applications.

In standard BOT or DBT problem, signal propagation interval is neglected under the assumption that the signal transmitting speed is much larger than the target speed. In this sense, the target remains its signal emitting position when the signal is received by the observer. However, it does not hold true in many practical applications. For instance, in passive sonar system, the target speed is sometimes comparable to the signal transmitting speed, thus the signal propagation interval can not be neglected and the target will travel to a different position when the signal is eventually received by the observer. Therefore, notable errors will occur between estimated target positions and true target positions if not taking signal time delay into consideration. Meanwhile, the interval between two consecutive signal emitting time points (so-called signal emitting interval or SEI for short) becomes unknown and time varying. This makes the traditional BOT methods inapplicable.

To solve this problem, an online parameter estimation method (OPE) is proposed in [16] to recursively compute the signal emitting intervals. It considers the SEI as a parameter and calculates it using linear search method before filtering stage. Once the SEI is determined, it becomes a standard BOT or DBT problem and some conventional algorithms can be applied. The OPE method can be embedded in nonlinear filters to recursively estimate the target state with delayed measurements. However, this OPE method can not be directly applied to a maneuvering target tracking problem since there is not an explicit system function in such case.

A popular way for describing maneuvering target dynamics is multiple model (MM) method [11, 22, 23]. The interactive multiple model (IMM) estimator [17, 18] is one of the most efficient dynamic MM estimators [16]. Various nonlinear filtering algorithms can run in the IMM framework. Some IMM filtering approach have been well developed, such as IMM-EKF, IMM-UKF, etc. [12, 13, 19] Particle filter (PF) [11, 24–26, 29] handles the problems with nonlinear dynamic and measurement equations better than (extended) Kalman filters, besides it can also be applied when the noises are non-Gaussian. A combination of the conventional IMM algorithm and PF is a novel

method [20, 30, 31].

Here a combined method named ISE-IMM is proposed to solve the signal time-delayed maneuvering target tracking problem. The iterative state estimation (ISE) method forms a general framework which controls the procedure of IMM filtering by updating the input value of SEI iteratively until an optimization termination is achieved; the IMM estimator is used to describe the posterior density of the maneuvering target state after a merging and filtering process. Since ISE-IMM method outputs a non-real-time relative state based on delayed measurements, a correction stage is added to estimate the current state of the target.

In this paper, the preferred nonlinear filtering method for an implementation of ISE-IMM algorithm is PF. Because the general PF algorithm needs some modifications to suit the IMM framework, an IMM-PF algorithm with an effective reducing resampling method is described in detail. This resampling method is based on the residual resampling method [34] and featured in roughening [26, 27].

The rest of this paper is organized as follows. Section 2 formulates the mathematical models for maneuvering target DBT with signal time delay. Section 3 proposes the general ISE method, ISE-IMM method and current state prediction method; some problems in special tracking scenarios are also discussed. In Section 4, some IMM filtering algorithms especially IMM-PF is introduced. Simulations and conclusions are presented in Sections 5 and 6, respectively.

2. MATHEMATIC MODELS FOR TIME-DELAYED TMA

2.1. Problem Description

In Figure 1, the observer receives a signal λ_{kT} at sample time kT which was originally emitted by the target at time $kT - t_k$, here t_k denotes the signal propagation interval. The target signal emitting position and current position are denoted as p_{kT-t_k} and p_{kT}, respectively. The interval $\Delta T_{k,k+1}$ between consecutive signal emitting time is referred to as "signal emitting interval" (SEI). For standard TMA, the SEI remains constant and is equal to observer sample interval T. But here it becomes unknown and time varying which depends on the tracking geometry.

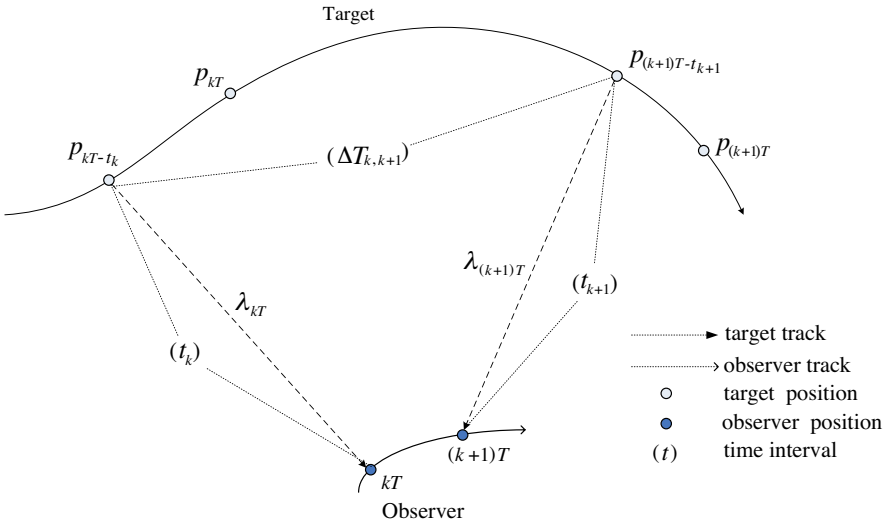

Figure 1. Illustration of TMA with signal time delay.

2.2. Mathematical Models

2.2.1. Target State Expression

The problem is mathematically defined in two dimensional Cartesian coordinates. At observer sample time kT, the target state vector is denoted as $\mathbf{x}_{kT}^t$. Let (x_{kT}^t, y_{kT}^t) be the target position and $(\dot{x}_{kT}^t, \dot{x}_{kT}^t)$ be the target velocity in the x-y plane. The target state vector is defined as

$$\mathbf{x}_{kT}^t = \left[x_{kT}^t, y_{kT}^t, \dot{x}_{kT}^t, \dot{x}_{kT}^t\right]^T \tag{1}$$

similarly, the observer state vector at time kT is

$$\mathbf{x}_{kT}^o = \left[x_{kT}^o, y_{kT}^o, \dot{x}_{kT}^o, \dot{x}_{kT}^o\right]^T \tag{2}$$

the relative state vector at time kT is then defined as

$$\mathbf{x}_{kT} = \mathbf{x}_{kT}^t - \mathbf{x}_{kT}^o = \left[x_{kT}, y_{kT}, \dot{x}_{kT}, \dot{x}_{kT}\right]^T \tag{3}$$

When taking the signal emitting time delay into consideration, suppose a signal is emitted by the target at time $kT - t_k$ (target state $\mathbf{x}_{kT-t_k}^t$) and received by the observer at time kT (target state $\mathbf{x}_{kT}^o$). Define the signal emitting state vector

$$\mathbf{x}_{kT-t_k,kT} = \mathbf{x}_{kT-t_k}^t - \mathbf{x}_{kT}^o \tag{4}$$

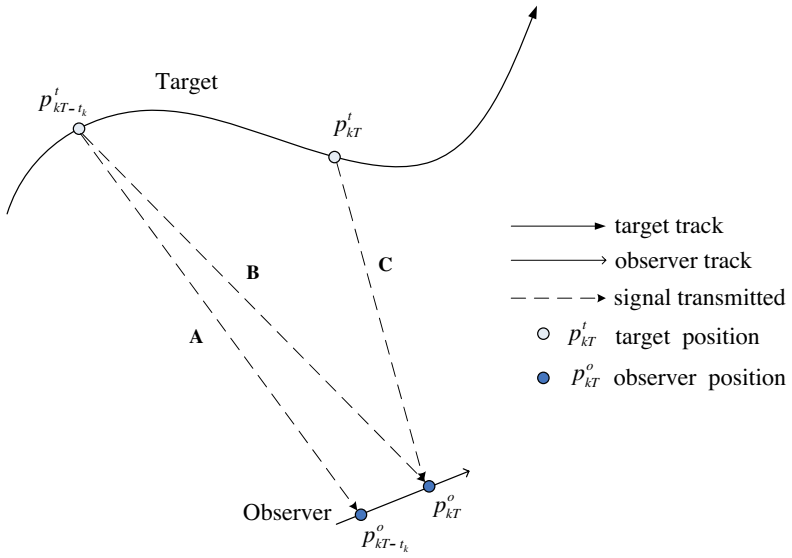

Figure 2. Illustration of time-delayed signal propagation.

Note in situation illustrated in Figure 2, vector $\mathbf{x}_{kT-t_k,kT}$ contains a position component **B**, rather than **A** or **C**. This means the observer always receives time-delayed signals which can not reflect the current states of the target.

2.2.2. Dynamic Models and Measurement Equations

The dynamics of a maneuvering target can be modeled by multiple switching regimes [11, 12]. Assume that during any observation interval T, the target obeys one of three dynamic models: (1) constant velocity (CV) motion model; (2) anticlockwise coordinated turn (CT) model; (3) clockwise CT model. Target dynamic model switches whenever it maneuvers. Let $r_k \in \{1, 2, 3\}$ be the mode variable denoting the target dynamic model in the interval $((k-1)T, kT]$.

Under the assumption that target remains its dynamic model unchanged in the interval $((k-1)T, kT]$, it is still possible for the target to experience more than one dynamic models within a single signal emitting interval. A typical situation is shown in Figure 3, where the target changes its dynamic mode from mode 1 to 3 during signal emitting interval $(3T - t_3, 4T - t_4]$. Obviously the target dynamics can not be simply described by any of three models in such a situation. However, in this paper, we are only interested in signal emitting state

at the end of every SEI and it can be well estimated after an IMM output merge step. This method will be described in Section 4. Here for simplicity, we can still assume target maintain its dynamic mode unchanged within a SEI. Let mode variable $r'_k \in \{1,2,3\}$ denotes the target dynamic model in the interval $((k-1)T - t_{k-1}, kT - t_k]$, then the target dynamics with signal time delay can be written as

$$\begin{aligned}\mathbf{x}_{(k+1)T-t_{k+1},(k+1)T} &= f\left(\mathbf{x}_{kT-t_k}, \mathbf{x}^o_{kT}, \mathbf{x}^o_{(k+1)T}, r'_{k+1}, \Delta T_{k,k+1}\right) + \Gamma_k \mathbf{v}_k \\ &= \mathbf{F}^{\left(r'_{k+1}\right)}\left(\mathbf{x}_{kT-t_k}, \Delta T_{k,k+1}\right) \cdot \left(\mathbf{x}_{kT-t_k} + \mathbf{x}^o_{kT}\right) \\ &\quad -\mathbf{x}^o_{(k+1)T} + \Gamma_k \mathbf{v}_k \end{aligned} \tag{5}$$

Here $\mathbf{F}^{(r'_{k+1})}(\cdot)$ is the transition matrix corresponding to mode variable r'_{k+1}. For this particular problem of interest, they can be specified as follows [12]. $\mathbf{F}^{(1)}(\cdot)$ corresponds to CV motion, $\mathbf{F}^{(2)}(\cdot)$ and $\mathbf{F}^{(3)}(\cdot)$ correspond to coordinated turn transitions (anticlockwise and clockwise, respectively). They are given by

$$\mathbf{F}^{(j)}(\mathbf{x}_{kT-t_k}, kT) =$$

$$\begin{cases} \begin{bmatrix} 1 & 0 & \Delta T_{k,k+1} & 0 \\ 0 & 1 & 0 & \Delta T_{k,k+1} \\ 0 & 0 & 1 & 0 \\ 0 & 0 & 0 & 1 \end{bmatrix}, j = 1 \\ \begin{bmatrix} 1 & 0 & \frac{\sin\left(\Omega^{(j)}_k \Delta T_{k,k+1}\right)}{\Omega^{(j)}_k} & -\frac{\left(1-\cos\left(\Omega^{(j)}_k \Delta T_{k,k+1}\right)\right)}{\Omega^{(j)}_k} \\ 0 & 1 & \frac{\left(1-\cos\left(\Omega^{(j)}_k \Delta T_{k,k+1}\right)\right)}{\Omega^{(j)}_k} & \frac{\sin\left(\Omega^{(j)}_k \Delta T_{k,k+1}\right)}{\Omega^{(j)}_k} \\ 0 & 0 & \cos\left(\Omega^{(j)}_k \Delta T_{k,k+1}\right) & -\sin\left(\Omega^{(j)}_k \Delta T_{k,k+1}\right) \\ 0 & 0 & \sin\left(\Omega^{(j)}_k \Delta T_{k,k+1}\right) & \cos\left(\Omega^{(j)}_k \Delta T_{k,k+1}\right) \end{bmatrix}, \ j = 2,3 \end{cases} \tag{6}$$

where the mode-conditioned turning rates are

$$\begin{aligned} \Omega^{(2)}_k &= \frac{a_m}{\sqrt{\left(\dot{x}_{kT-t_k,kT} + \dot{x}^o_{kT}\right)^2 + \left(\dot{y}_{kT-t_k,kT} + \dot{y}^o_{kT}\right)^2}} \\ \Omega^{(3)}_k &= -\frac{a_m}{\sqrt{\left(\dot{x}_{kT-t_k,kT} + \dot{x}^o_{kT}\right)^2 + \left(\dot{y}_{kT-t_k,kT} + \dot{y}^o_{kT}\right)^2}} \end{aligned} \tag{7}$$

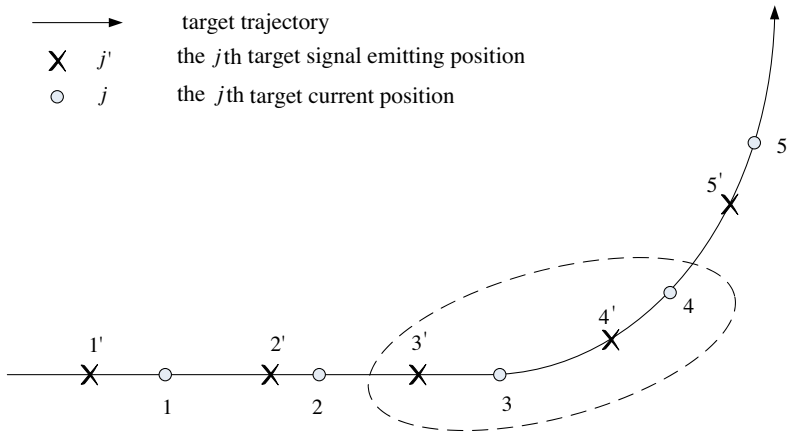

Figure 3. Target changes its dynamic model during SEI.

Here a_m is a typical maneuver acceleration. Since the turning rate is time variant and expressed as a nonlinear function of target speed, mode 2, 3 are clearly nonlinear transformations. Γ_k is given by

$$\Gamma_k = \begin{bmatrix} \Delta T_{k,k+1}^2/2 & 0 \\ 0 & \Delta T_{k,k+1}^2/2 \\ \Delta T_{k,k+1} & 0 \\ 0 & \Delta T_{k,k+1} \end{bmatrix} \tag{8}$$

$\mathbf{v}_k$ is a 2×1 i.i.d. process noise with zero mean and covariance $\mathbf{Q} = \sigma_a^2 \mathbf{I}_2$. Here $\mathbf{I}_2$ is a 2×2 identity matrix.

Here available measurements are signal frequency and the angle from the target to the observer, referenced to the y-axis. Suppose the target emits single frequency f_0 tonal signal during observation time, the received signal frequency at kT is z_{kT}^f, the measured angle is z_{kT}^θ, the measurement equation can be expressed as

$$\mathbf{z}_{kT} = h\left(\mathbf{x}_{kT-t_k,kT}, \mathbf{x}_{kT}^o\right) + \boldsymbol{\omega}_k \tag{9}$$

or

$$\begin{bmatrix} z_{kT}^\theta \\ z_{kT}^f \end{bmatrix} = \begin{bmatrix} \arctan\left(\dfrac{x_{kT-t_k}}{y_{kT-t_k}}\right) \\ f_0 \cdot \dfrac{v_s + \rho_{kT-t_k}^{(1)}}{v_s + \rho_{kT-t_k}^{(2)}} \end{bmatrix} + \begin{bmatrix} \omega_k^\theta \\ \omega_k^f \end{bmatrix} \tag{10}$$

where

$$\rho^{(1)}_{kT-t_k}=\frac{\dot{x}^o_{kT}\cdot x_{kT-t_k,kT}+\dot{y}^o_{kT}\cdot y_{kT-t_k,kT}}{\sqrt{x^2_{kT-t_k}+y^2_{kT-t_k,kT}}}$$
$$\rho^{(2)}_{kT-t_k}=\frac{(\dot{x}^o_{kT}+\dot{x}_{kT-t_k,kT})\cdot x_{kT-t_k,kT}+(\dot{y}^o_{kT}+y_{kT-t_k,kT})\cdot y_{kT-t_k,kT}}{\sqrt{x^2_{kT-t_k}+y^2_{kT-t_k,kT}}} \quad (11)$$

according to Doppler effect equation. $\boldsymbol{\omega}_k$ is a zero-mean Gaussian white noise with covariance $\mathbf{R}_k = \mathrm{diag}(\sigma^2_\theta, \sigma^2_f)$; v_s is the signal transmit velocity. The objective of DBT with signal time delay is to estimate $\hat{\mathbf{x}}_{kT} = \mathbb{E}(\mathbf{x}_{kT} \mid \mathbf{z}_{kT})$ out of noise corrupted, time-delayed signals.

For BOT problem, the only difference lies in the measurement function where BOT only has bearing measurements.

If the time varying signal emitting interval $\Delta T_{k,k+1}$ is replaced by constant sample interval T, it becomes standard DBT or BOT problem. Compare signal-time-delayed DBT problem with standard DBT problem, we find the former is more complicated: both the dynamic and measurement equations are functions of delayed state vector $\mathbf{x}_{kT-t_k,kT}$ rather than current state vector $\mathbf{x}_{kT}$. Moreover, the value of SEI is unknown and time varying. The methods to solve these problems are introduced in Section 3.

3. SIGNAL TIME DELAY ANALYSIS

Estimation of SEI is a major task of TMA with signal time delay. In Section 3.1, an iterative state estimation (ISE) method is proposed to estimate the SEI as well as target state in every sample interval, with known target dynamic model. Section 3.2 extends the ISE method to solve maneuvering target TMA with multi-model dynamics. Section 3.3 presents a method to predict the current state based on the estimation of signal emitting state. Some interesting cases are discussed in Section 3.4.

3.1. Iterative State Estimation Method

Suppose the estimation of last-step signal emitting state vector at kT is given as

$$\hat{\mathbf{x}}_{kT-t_k,kT} = \mathbb{E}\left(\mathbf{x}_{kT-t_k,kT} \mid \mathbf{z}_{kT}\right) \quad (12)$$

Assume the target current dynamic mode is known as r'_{k+1}, the objective of current step is to predict $\hat{\mathbf{x}}_{(k+1)T-t_{k+1},(k+1)T}$ based on

$\hat{\mathbf{x}}_{kT-t_k,kT}$ and measurement $\mathbf{z}_{(k+1)T}$. The signal time delay equation can be derived from Figure 1:

$$\Delta T_{k,k+1} + t_{k+1} = T + t_k \tag{13}$$

After moving t_{k+1} to the right side of the equation, the SEI is expressed as:

$$\Delta T_{k,k+1} = T - t_{k+1} + t_k \tag{14}$$

It also holds true for the estimated values:

$$\Delta \hat{T}_{k,k+1} = T - \hat{t}_{k+1} + \hat{t}_k \tag{15}$$

Here the sample interval T is a constant, signal propagation interval $\hat{t}_k$ is known from previous calculation. Therefore $\Delta \hat{T}_{k,k+1}$ is a function of $\hat{t}_{k+1}$. For simplicity, we denote the function as

$$\Delta \hat{T}_{k,k+1} = \varphi\left(\hat{t}_{k+1}\right) \tag{16}$$

Signal propagation interval $\hat{t}_{k+1}$ is determined by the signal emitting state vector $\hat{\mathbf{x}}_{(k+1)T-t_{k+1},(k+1)T}$ which contains the relative position components. It is given by

$$\hat{t}_{k+1} = \frac{\sqrt{\hat{x}^2_{(k+1)T-t_{k+1},(k+1)T} + \hat{y}^2_{(k+1)T-t_{k+1},(k+1)T}}}{v_s} \tag{17}$$

where v_s is the signal transmitting velocity.

The calculation of $\hat{\mathbf{x}}_{(k+1)T-t_{k+1},(k+1)T}$ is based on a recursive nonlinear filter algorithm (EKF, UKF, PF, etc.). For simplicity, here we denote the functional relationship as

$$\hat{\mathbf{x}}_{(k+1)T-t_{k+1},(k+1)T} = \zeta\left(\Delta \hat{T}_{k,k+1}, \hat{\mathbf{x}}_{kT-t_k,kT}, r'_{k+1}, \mathbf{z}_{(k+1)T}\right) \tag{18}$$

where mode variable r'_{k+1} and measurements $\mathbf{z}_{(k+1)T}$ are assumed to be known, $\hat{\mathbf{x}}_{kT-t_k,kT}$ is obtained from the last cycle. Thus $\hat{\mathbf{x}}_{(k+1)T-t_{k+1},(k+1)T}$ can be calculated if and only if $\Delta \hat{T}_{k,k+1}$ is given.

Combining Equations (17) and (18), we can find that $\hat{t}_{k+1}$ is a function of $\Delta \hat{T}_{k,k+1}$, which can be denoted as

$$\hat{t}_{k+1} = \psi\left(\Delta \hat{T}_{k,k+1}\right) \tag{19}$$

Therefore, the problem is to find an appropriate value of $\hat{T}_{k,k+1}$ to satisfy both Equations (16) and (19) such as

$$\begin{cases} \Delta\hat{T}_{k,k+1} = \varphi\left(\hat{t}_{k+1}\right) \\ \hat{t}_{k+1} = \psi\left(\Delta\hat{T}_{k,k+1}\right) \end{cases} \tag{20}$$

In practice, this can be changed into the following optimization problem

$$\begin{cases} \left|\Delta\hat{T}_{k,k+1} - \varphi(\hat{t}_{k+1})\right| \leq \delta \\ s.t. \;\; \hat{t}_{k+1} = \psi\left(\Delta\hat{T}_{k,k+1}\right) \end{cases} \tag{21}$$

where δ is chosen as a optimization threshold parameter.

A way to solve the problem is linear search method proposed in [16], but it may be computational expensive when Equation (18) is very complex. The predefined increment must be small enough to ensure the optimization solution exists. With a smaller increment, the result is expected to be more precise, but accompanied with a rise in total search steps.

For linear search method, it's necessary to define searching bounds to guarantee termination of the algorithm [16]. The searching bounds are related with the last-step target state. However, strict constraints on the signal emitting interval may deteriorate the performance of tracking algorithm, especially when the previous target state estimation is inaccurate. In such a situation, the estimated SEI is very likely to be out of bounds in order to keep track with the true trajectory.

Therefore, we proposed an iterative method to deal with the problem. Assume at time step k, the estimated state is $\hat{\mathbf{x}}_{kT-t_k}$, the signal propagation interval is $\hat{t}_k$, the signal emitting interval is $\Delta\hat{T}_{k-1,k}$. The mode variable at step $k+1$ is r'_{k+1}. The initial estimated value of $\Delta\hat{T}_{k,k+1}$ is set to be

$$\Delta\hat{T}^{(\alpha)}_{k,k+1} = \Delta\hat{T}_{k-1,k} \tag{22}$$

Then the initial estimation of signal emitting state vector $\hat{\mathbf{x}}^{(\beta)}_{(k+1)T-t_k,(k+1)T}$ can be calculated according to Equation (18). It is rewritten here as follows:

$$\hat{\mathbf{x}}^{(\beta)}_{(k+1)T-t_k,(k+1)T} = \zeta\left(\Delta\hat{T}^{(\alpha)}_{k,k+1}, \hat{\mathbf{x}}_{kT-t_k,kT}, r'_{k+1}, \mathbf{z}_{(k+1)T}\right) \tag{23}$$

The propagation interval is:

$$\hat{t}_{k+1}^{(\beta)} = \frac{\sqrt{\left(\hat{x}^{(\beta)}_{(k+1)T-t_{k+1},(k+1)T}\right)^2 + \left(\hat{y}^{(\beta)}_{(k+1)T-t_{k+1},(k+1)T}\right)^2}}{v_s} \tag{24}$$

Then an approximation of $\Delta\hat{T}_{k,k+1}$ is given by

$$\Delta\hat{T}_{k,k+1}^{(\beta)} = \varphi(\hat{t}_{k+1}^{(\beta)}) = T - \hat{t}_{k+1}^{(\beta)} + \hat{t}_k \tag{25}$$

Substitute $\Delta\hat{T}_{k,k+1}^{(\alpha)}$ and $\Delta\hat{T}_{k,k+1}^{(\beta)}$ into

$$\left|\Delta\hat{T}_{k,k+1}^{(\alpha)} - \Delta\hat{T}_{k,k+1}^{(\beta)}\right| \leq \delta \tag{26}$$

to test whether it holds. If not, update $\Delta\hat{T}_{k,k+1}^{(\alpha)}$ by $a\cdot\Delta\hat{T}_{k,k+1}^{(\alpha)}+(1-a)\cdot\Delta\hat{T}_{k,k+1}^{(\beta)}$, where a is a positive number between 0 and 1. For simplicity, it can be set to 0.5. Repeat Equations (23)–(25) until Equation (26) becomes true, then output approximations of signal emitting state vector $\hat{\mathbf{x}}_{(k+1)T-t_{k+1},(k+1)T}$ and SEI $\Delta\hat{T}_{k,k+1}$. To avoid endless iterations when a divergent case occurs, the maximum count of iterative cycles is set to m.

The pseudocodes of the iterative state estimation (ISE) method is described in Table 1.

3.2. Maneuvering Target Tracking with Signal Time Delay

3.2.1. The Interactive Multiple Model Estimator

The IMM estimator [18, 21], with the Markov switching coefficient, is one of the most efficient dynamic multiple model estimators. All dynamic models are parallel processed and the model probability represent model switch. Some implementations of IMM filters are presented in Section 4.

3.2.2. ISE-IMM Method

IMM estimator can be easily embedded into ISE method if we replace the function $\zeta(\cdot)$ in Equation (18) by an IMM estimator: in this way signal emitting state vector can be estimated step by step. The structure of ISE-IMM method is described in Figure 4, where $j \in \{1, 2, 3\}$ denotes the different modes.

Table 1. Iterative State Estinmation (ISE).

$\left[\Delta\hat{T}_{k,k+1}, \hat{t}_{k+1}, \hat{\mathbf{x}}_{(k+1)T-t_{k+1},(k+1)T}\right] = ISE\left[\Delta\hat{T}_{k-1,k}, \hat{t}_k, \hat{\mathbf{x}}_{kT-t_k,kT}, r'_{k+1}, m\right]$

- Initialize $\Delta\hat{T}^{(\alpha)}_{k,k+1} = \Delta\hat{T}_{k-1,k}$; set $step = 1$
- Calculate $\hat{\mathbf{x}}^{(\beta)}_{(k+1)T-t_{k+1},(k+1)T}$ using Equation (23)
- Calculate $\hat{t}^{(\beta)}_{k+1}$ using Equation (24)
- Calculate $\Delta\hat{T}^{(\beta)}_{k,k+1}$ using Equation (25)
- WHILE $\left|\Delta\hat{T}^{(\beta)}_{k,k+1} - \Delta\hat{T}^{(\alpha)}_{k,k+1}\right| > \delta$ AND $step \leq m$
  - Update $\Delta\hat{T}^{(\alpha)}_{k,k+1}$ By $a\cdot\Delta\hat{T}^{(\alpha)}_{k,k+1} + (1-a)\cdot\Delta\hat{T}^{(\beta)}_{k,k+1}$ $(0 < a < 1)$
  - Calculate $\hat{\mathbf{x}}^{(\beta)}_{(k+1)T-t_{k+1},(k+1)T}$ using Equation (23)
  - Calculate $\hat{t}^{(\beta)}_{k+1}$ using Equation (24)
  - Calculate $\Delta\hat{T}^{(\beta)}_{k,k+1}$ using Equation (25)
  - $step = step + 1$
- END WHILE
- Assign $\Delta\hat{T}_{k,k+1} = \hat{T}^{(\beta)}_{k,k+1}$
- Assign $\hat{t}_{k+1} = \hat{t}^{(\beta)}_{k+1}$
- Assign $\hat{\mathbf{x}}_{(k+1)T-t_{k+1},(k+1)T} = \hat{\mathbf{x}}^{(\beta)}_{(k+1)T-t_{k+1},(k+1)T}$

3.3. Target Current State Prediction

In Figure 4, the output of each step k is the estimation of signal emitting state vector $\mathbf{x}_{kT-t_k,kT}$, which is denoted as $\hat{\mathbf{x}}_{kT-t_k,kT}$, and $\hat{\mathbf{x}}_{kT-t_k,kT} = \mathbb{E}(\mathbf{x}_{kT-t_k,kT} \mid \mathbf{z}_{kT})$. However, the eventual objective of TMA with signal time delay is to estimate the state vector $\hat{\mathbf{x}}_{kT}$ at sample time kT, where $\hat{\mathbf{x}}_{kT} = \mathbb{E}(\mathbf{x}_{kT} \mid \mathbf{z}_{kT})$. The target current state estimation $\hat{\mathbf{x}}^t_{kT}$ is given by:

$$\hat{\mathbf{x}}^t_{kT} = \mathbf{x}^o_{kT} + \hat{\mathbf{x}}_{kT} \tag{27}$$

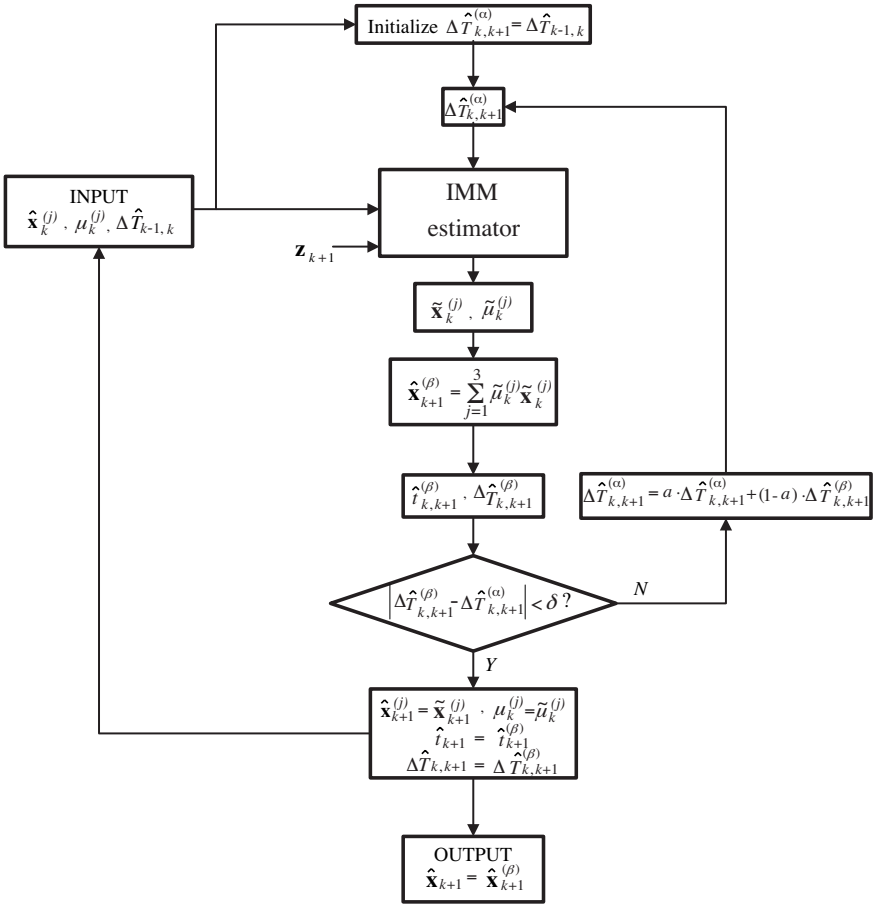

Figure 4. Structure of ISE-IMM method.

Since there is not any direct information about the target current state, $\hat{\mathbf{x}}_{kT}$ can only be predicted according to the estimated state vector $\hat{\mathbf{x}}_{kT-t_k,kT}$ and signal propagation time $\hat{t}_k$. The prediction of current relative state is expressed as

$$\hat{\mathbf{x}}_{kT}=\sum_{j=1}^{3}\mu_k^{(j)}\cdot\left[\mathbf{F}^{(j)}(\hat{\mathbf{x}}_{kT-t_k,kT},\hat{t}_k)\cdot(\hat{\mathbf{x}}_{kT-t_k,kT}+\mathbf{x}^o_{kT})-\mathbf{x}^o_{kT}\right] \quad (28)$$

where $\mu_k^{(j)}$ denotes the normalized probability of mode j at step k, $\hat{t}_k$ is the estimated signal propagation time, both are outputs of ISE-IMM method.

3.4. Mode Switch Error in Prediction Stage

Using prediction method mentioned above, the real-time state $\hat{x}_{kT}$ can be estimated based on the time-delayed state $\hat{x}_{kT-t_k}$. However, there are some circumstances under which the real-time trajectory is unpredictable. Considering the tracking scenario in Figure 5:

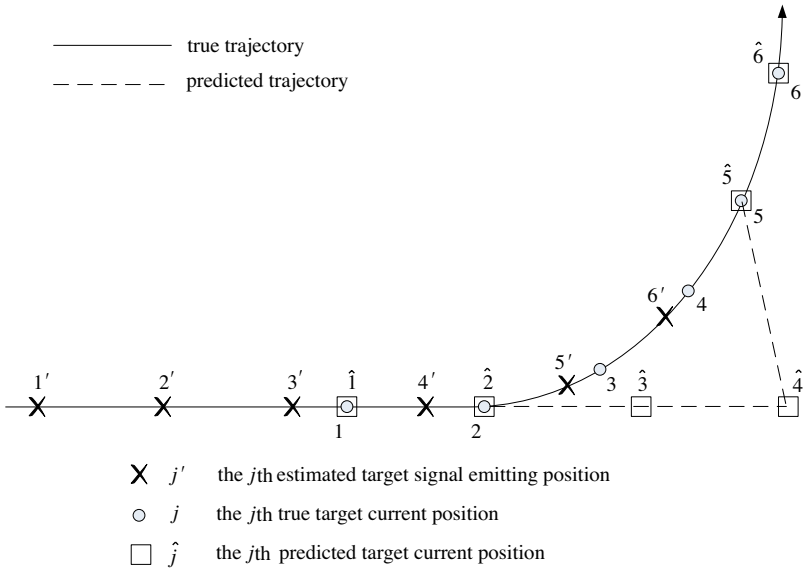

Figure 5. Mode switch error in a tracking scenario.

In Figure 5, six consecutive sample intervals are taken from the observation period. Suppose we have a perfect estimation so that estimated values of state $\hat{\mathbf{x}}_{kT-t_k}$, mode probability $\mu_k^{(j)}$ and signal propagation interval $\hat{t}_k$ are equal to true values. Under such assumption, the first two predicted positions perfectly match the true ones since the target remains the CV model during signal propagation interval. But this is not the case for the 3rd and 4th sample intervals. When the 3rd sample state is on the turning, signal reflecting $\hat{\mathbf{x}}_{3T-t_3}$ arrived at the observer, then the ISE-IMM method tells the most probable motion mode is CV. A prediction is made according to the wrong mode probability thus big error occurs at the turning. We call the error mode switch error. In the 5th sample interval, target signal emitting state and current state are in the same dynamic mode again, so the predicted position is true.

Generally speaking, the mode switch error occurs when the following two conditions are both satisfied: (1) $t_k \geq T$; (2) $r'_k \neq r_k$.

So obviously there is no mode switch error in non-maneuvering case, where $r'_k = r_k = 1$ at any time step. If $t_k < T$ holds true in every sample interval as the case illustrated in Figure 6, there is no mode switch error either.

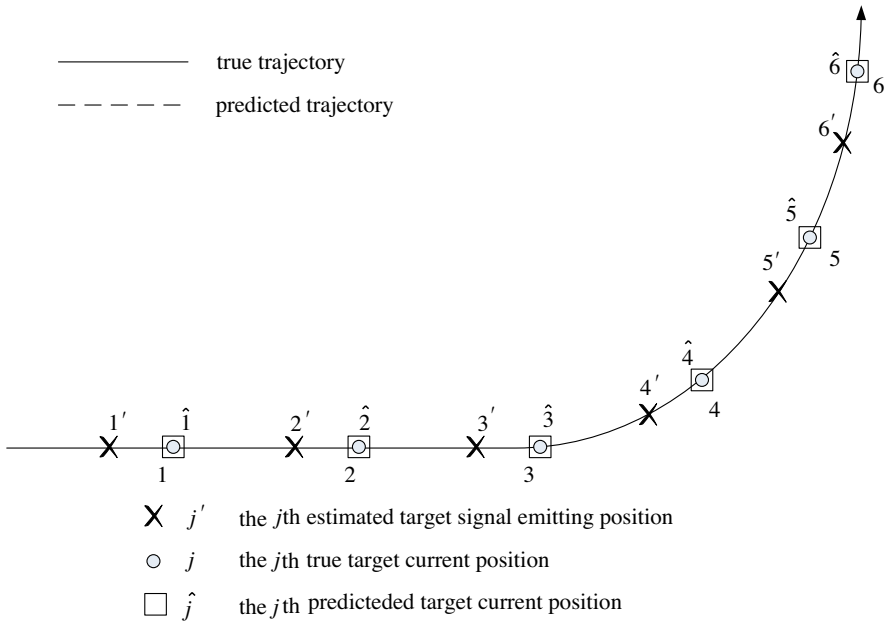

Figure 6. A tracking scenario without mode switch error.

By decreasing sample interval T, mode switch error can be reduced but by no means eliminated. Mode switch error potentially deteriorates the accuracy of current position estimation, but luckily it does not necessarily happen in every tracking scenario and only has effect on the beginning steps of mode switching.

4. IMM FILTER ALGORITHMS

IMM (interacting multiple model) algorithm is featured by its merging stage: the input to any of the model-matched filters is an interaction of all the model-matched filters. According to the dynamic model formulated in Section 2.2, three parallel model-matched filters are required for CV motion, clockwise and anticlockwise motion, respectively.

Theoretically, the model-matched filter in the framework of IMM algorithm can be implemented with any nonlinear filter algorithms.

But for particle filter (PF) the situation is slightly different, because PF uses a set of weighted particles rather than the mean and the covariance to describe a distribution. So the IMM algorithm needs to be modified to suit the case.

4.1. General IMM Algorithm

The IMM algorithm is developed under the assumption that the evolvement of mode variable r_k can be modeled by a Markov chain with transitional probability matrix $\mathbf{\Pi}$, where k is the time index. In the specified problem here,

$$\mathbf{\Pi}_{ij} \triangleq p\{r_k = j \mid r_{k-1} = i\}, \quad i, j \in \mathbb{M} \triangleq \{1, 2, 3\} \tag{29}$$

According to Section 2.2, the target motion is classified into three models. Thus $\mathbf{\Pi}$ is a 3×3 matrix with elements satisfying $\mathbf{\Pi}_{ij} \geq 0$ and $\sum_{j=1}^{3} \mathbf{\Pi}_{ij} = 1$. Sometimes such dynamics of the target is referred to as jump Markov system.

The general IMM algorithm can be implemented with any nonlinear filter which describes the probability density by mean and covariance, such as EKF and UKF. The basic idea is that for each dynamic model, a mode-matched filter is used, and the filter outputs are weighted according to the mode probabilities to give the estimations of state mean and covariance. At each time index, the target state pdf is characterized by a finite Gaussian mixture which is then propagated to the next time index [12]. Details of the general IMM algorithm can be found in [17]; an algorithm summary of IMM-EKF is presented in [22].

4.2. IMM-PF Algorithm

The IMM-PF cycle has the following stages.
1. Input interaction stage:

$$\begin{aligned} &\left[\left\{\mathbf{x}_{k-1}^{(i,n)}, r_{k-1}^{(i,n)}, w_{k-1}^{(i,n)}\right\}, i \in \mathbb{M}, n \in \mathbb{S}\right] \\ \rightarrow &\left[\left\{\mathbf{x}_{k-1}^{(i,n)(j)}, r_{k-1}^{(i,n)(j)}, w_{k-1}^{(i,n)(j)}\right\}, \ i, j \in \mathbb{M}, n \in \mathbb{S}\right] \end{aligned} \tag{30}$$

where $\mathbb{M} \triangleq \{1, 2, 3\}$ denotes the set of mode variables and $\mathbb{S} \triangleq \{1, 2, \ldots, N\}$ is the set of particle indices. Each mode has N particles.

At time index $k-1$, the IMM-PF starts with a set of $3N$ weighted

particles, with mode variable $r_{k-1}^{(i,n)} = i$, and weights satisfying

$$\sum_{i=1}^{3}\sum_{n=1}^{N} w_{k-1}^{(i,n)} = 1,\ i \in \mathbb{M}, n \in \mathbb{S} \tag{31}$$

Note for each mode $r_{k-1} = i$, N weighted particles span the empirical density

$$p_{\mathbf{x}_{k-1}|r_{k-1},\mathbf{z}_{k-1}}(\mathbf{x}|\, r_{k-1} = i) = \sum_{n=1}^{N} w_{k-1}^{(i,n)} \delta\left(\mathbf{x} - \mathbf{x}_{k-1}^{(i,n)}\right) \Bigg/ \sum_{n=1}^{N} w_{k-1}^{(i,n)} \tag{32}$$

as an approximation of the exact density.

After the interaction stage, the conditional probability density for mode $r_k = j$ changes into

$$\begin{aligned}\tilde{p}_{\mathbf{x}_{k-1}|r_k,\mathbf{z}_{k-1}}(\mathbf{x} \mid r_k = j) &= \sum_{i=1}^{3}\left[\mathbf{\Pi}_{ij}\sum_{n=1}^{N} w_{k-1}^{(i,n)}\delta\left(\mathbf{x} - \mathbf{x}_{k-1}^{(i,n)}\right)\right] \Bigg/ \tilde{w}_{k-1}^{(j)} \\ &= \sum_{i=1}^{3}\sum_{n=1}^{N} \mathbf{\Pi}_{ij} w_{k-1}^{(i,n)}\delta\left(\mathbf{x} - \mathbf{x}_{k-1}^{(i,n)}\right) \Bigg/ \tilde{w}_{k-1}^{(j)}\end{aligned} \tag{33}$$

where

$$\tilde{w}_{k-1}^{(j)} = \sum_{i=1}^{3}\sum_{n=1}^{N} \mathbf{\Pi}_{ij} w_{k-1}^{(i,n)} \tag{34}$$

serves as a normalization factor, or an approximation of mode probability $\tilde{p}_{r|\mathbf{z}_{k-1}}(r_k = j)$ after interaction stage.

According to Equation (33), density $\tilde{p}_{\mathbf{x}_{k-1}|r_k,\mathbf{z}_{k-1}}(\mathbf{x} \mid r_k = j)$ is spanned by $3N$ weighted particles denoted as

$$\left\{\mathbf{x}_{k-1}^{(i,n)(j)}, r_{k-1}^{(i,n)(j)}, w_{k-1}^{(i,n)(j)}\right\},\ i \in \mathbb{M}, n \in \mathbb{S} \tag{35}$$

where

$$\begin{aligned}\mathbf{x}_{k-1}^{(i,n)(j)} &= \mathbf{x}_{k-1}^{(i,n)} \\ r_{k-1}^{(i,n)(j)} &= r_{k-1}^{(i,n)} = j \\ w_{k-1}^{(i,n)(j)} &= \mathbf{\Pi}_{ij} w_{k-1}^{(i,n)} / \tilde{w}_{k-1}^{(j)}\end{aligned} \tag{36}$$

2. Resampling stage

$$\begin{aligned}&\left[\left\{\mathbf{x}_{k-1}^{(i,n)(j)}, r_{k-1}^{(i,n)(j)}, w_{k-1}^{(i,n)(j)}\right\},\ i,j \in \mathbb{M}, n \in \mathbb{S}\right] \\ \rightarrow &\left[\left\{\tilde{\mathbf{x}}_{k-1}^{(j,n)}, \tilde{r}_{k-1}^{(j,n)}, \tilde{w}_{k-1}^{(j,n)}\right\},\ j \in \mathbb{M}, n \in \mathbb{S}\right]\end{aligned} \tag{37}$$

In order to maintain the fixed number of particles per mode, a resampling stage is necessary after the input interaction. In this paper, residual resampling algorithm is applied combined with a roughening procedure [26–28]. An independent jitter $\mathbf{c}_{k-1}^{(i,n)(j)}$ is added to each sample $\mathbf{x}_{k-1}^{(i,n)(j)}$. In practice, this method can effectively boost the diversity of particles without significantly increasing computational complexity.

After roughening, residual sampling which reduces the number of particles from $3N$ to N is implemented as follows:
(a) For mode j, denote

$$\left\{\mathbf{x}_{k-1}^{(i,n)(j)} + \mathbf{c}_{k-1}^{(i,n)(j)}, r_{k-1}^{(i,n)(j)}, w_{k-1}^{(i,n)(j)}\right\} = \left\{\mathbf{x}_{k-1}^{(j,m)}, r_{k-1}^{(j,m)}, w_{k-1}^{(j,m)}\right\} \quad (38)$$

where $m = N(i-1)+n$, hence $m \in \{1, 2, 3 \cdots, 3N\}$. Then retain $l_{k-1}^{(j,m)} = \lfloor N w_{k-1}^{(j,m)} \rfloor$ copies of sample $\mathbf{x}_{k-1}^{(j,m)}$. The total number of retained copies will not surpass N.
(b) Let $l_r^{(j)} = N - \sum_{m=1}^{3N} l_{k-1}^{(j,m)}$. If $l_r^{(j)} > 0$, obtain $l_r^{(j)}$ samples i.i.d. drawn from $\left\{\mathbf{x}_{k-1}^{(l,m)}\right\}$ with probabilities proportional to $N w_{k-1}^{(j,m)} - l_{k-1}^{(j,m)}$, $m = 1, 2, \ldots, 3N$.
(c) After steps (a) and (b), N samples have been drawn from $3N$ particles, and they form a set $\left\{\tilde{\mathbf{x}}_{k-1}^{(j,n)}, \tilde{r}_{k-1}^{(j,n)}, \tilde{w}_{k-1}^{(j,n)}\right\}$, $j \in \mathbb{M}, n \in \mathbb{S}$. Mode variable $\tilde{r}_{k-1}^{(j,n)} = j$. Particle weight $\tilde{w}_{k-1}^{(j,n)}$ is set to $\tilde{w}_{k-1}^{(j)}/N$, where $\tilde{w}_{k-1}^{(j)}$ is defined by Equation (34).
3. Prediction and correction stage

$$\begin{aligned} &\left[\left\{\tilde{\mathbf{x}}_{k-1}^{(i,n)}, \tilde{r}_{k-1}^{(i,n)}, \tilde{w}_{k-1}^{(i,n)}, \mathbf{z}_k\right\},\ i \in \mathbb{M}, n \in \mathbb{S}\right] \\ \rightarrow &\left[\left\{\mathbf{x}_k^{(i,n)}, r_k^{(i,n)}, w_k^{(i,n)}\right\},\ i \in \mathbb{M}, n \in \mathbb{S}\right] \end{aligned} \quad (39)$$

According to the system dynamic Equation (5), prediction step is applied as follows:

$$\mathbf{x}_k^{(i,n)} = f_{k-1}^{(i)}\left(\mathbf{x}_{k-1}^{(i,n)}\right) \quad (40)$$

mode variables remain unchanged in this stage, so

$$r_k^{(i,n)} = \tilde{r}_{k-1}^{(i,n)} = i \quad (41)$$

particle weight is updated according to

$$w_k^{(i,n)} = \frac{\tilde{w}_{k-1}^{(i,n)} \Lambda_k^{(i,n)}}{\sum_{i=1}^{3} \sum_{n=1}^{N} \tilde{w}_{k-1}^{(i,n)} \Lambda_k^{(i,n)}} \tag{42}$$

Here the likelihood $\Lambda_k^{(i,n)}$ is given by

$$\begin{aligned} \Lambda_k^{(i,n)} &= p\left(\mathbf{z}_k \mid \mathbf{x}_k^{(i,n)}, r_k^{(i,n)} = i\right) = \mathcal{N}\left(\boldsymbol{\upsilon}; 0, \mathbf{S}_k^{(i)}\right) \\ &= \frac{1}{2\boldsymbol{\pi}\left|\mathbf{S}_k^{(n)}\right|^{1/2}} \exp\left(-\frac{1}{2}\left(\boldsymbol{\upsilon}_k^{(i,n)}\right)^T \left(\mathbf{S}_k^{(n)}\right)^{-1} \boldsymbol{\upsilon}_k^{(i,n)}\right) \end{aligned} \tag{43}$$

where

$$\begin{aligned} \boldsymbol{\upsilon}_k^{(i,n)} &= \mathbf{z}_k - h_k\left(\mathbf{x}_k^{(i,n)}\right) \\ \tilde{\mathbf{z}}_k^{(n)} &= \sum_{i=1}^{N} \frac{1}{N} h_k\left(\mathbf{x}_k^{(i,n)}\right) \\ \mathbf{S}_k^{(n)} &= \sum_{i=1}^{N} \frac{1}{N}\left[h_k\left(\mathbf{x}_k^{(i,n)}\right) - \tilde{\mathbf{z}}_k^{(n)}\right]\left[h_k\left(\mathbf{x}_k^{(i,n)}\right) - \tilde{\mathbf{z}}_k^{(n)}\right]^T + \mathbf{R}_k \end{aligned} \tag{44}$$

4. Output stage
Merge the $3N$ samples into one final output estimate state:

$$\left[\left\{\mathbf{x}_k^{(i,n)}, r_k^{(i,n)}, w_k^{(i,n)}\right\},\ i \in \mathbb{M}, n \in \mathbb{S}\right] \rightarrow [\mathbf{x}_k] \tag{45}$$

Mode probability is approximated as

$$w_k^{(i)} = \sum_{n=1}^{N} w_k^{(i,n)} \tag{46}$$

For each mode, a model state vector is given by

$$\mathbf{x}_k^{(i)} = \sum_{n=1}^{N} w_k^{(i,n)} \mathbf{x}_k^{(i,n)} \Big/ w_k^{(i)} \tag{47}$$

And the final output is

$$\mathbf{x}_k = \sum_{i=1}^{3} w_k^{(i)} \mathbf{x}_k^{(i)} \tag{48}$$

Note the output of particle filter algorithm is the *a posteriori* probability density of the stage given all measurements. An estimate of the density is

$$p_{\mathbf{x}_k|r_k,\mathbf{z}_k}\left(\mathbf{x} \mid r_k = i\right) = \sum_{n=1}^{N} w_k^{(i,n)} \delta\left(\mathbf{x} - \mathbf{x}_k^{(i,n)}\right) \Big/ w_k^{(i)} \tag{49}$$

In next section we'll apply two kinds of IMM filters to solve a maneuvering target tracking problem with time delay.

5. SIMULATIONS

Suppose a fixed ground-based acoustic sensor is tracking a low altitude target. Figure 7 shows the configuration. Here the time step (or the sensor scan period) is $T = 5\,\mathrm{s}$ and the whole scenario lasts $400s$ (or 80 steps). Sound speed in air is 340 m/s. Target radiates single 300Hz tone and is known by the observer [33, 34]. The target starts from $(-1, 4)$. It maintains a constant speed of 351.7 km/h (or 0.0977 km/s) with an initial course of 83°. It executes the first maneuver from time step $k = 21$ to $k = 32$ and attains a new course of 207°. The second maneuver begins at time step $k = 45$ and lasts 12 steps, at the end the target attains a course of 96° and maintains the new course for

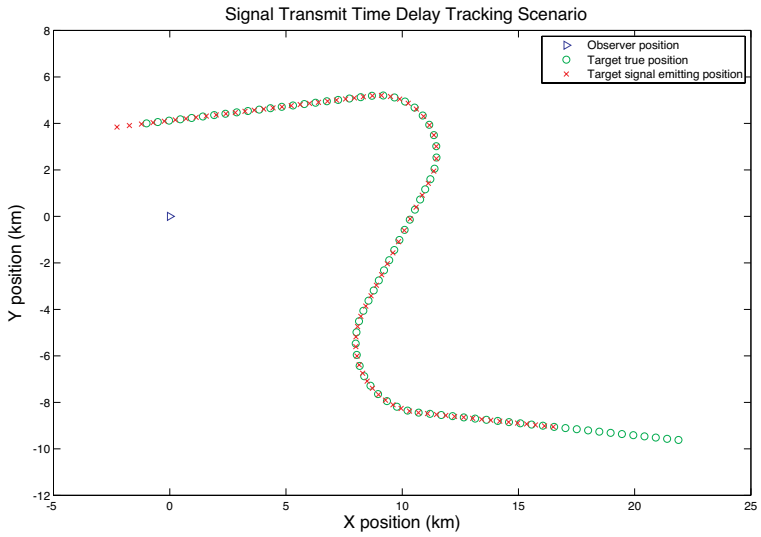

Figure 7. Signal time-delayed tracking scenario illustration.

the rest of the observation period. The maneuvering acceleration in two turnings are $0.0038, 0.0032\,\mathrm{km/s^2}$, respectively. The sensor is fixed at (0, 0), 4.123 km away from the initial position of the target. The measurement standard deviation is $\sigma_\theta = 0.0262\,\mathrm{rad}$ for bearing and $\sigma_f = 0.2\,\mathrm{Hz}$ for frequency. The process noise standard deviation is set to $\sigma_a = 1.6 \times 10^{-4}\,\mathrm{km/s^2}$.

The following parameters are used in simulation for filter initialization. The transition probability matrix required in the IMM method is set to be

$$\mathbf{\Pi} = \begin{bmatrix} 0.9 & 0.05 & 0.05 \\ 0.4 & 0.5 & 0.1 \\ 0.4 & 0.1 & 0.5 \end{bmatrix} \tag{50}$$

The initial speed and course standard deviations are set to $\sigma_s = 1 \times 10^{-4}\,\mathrm{km/s}$ and $\sigma_c = \pi/4\,\mathrm{rad}$. The initial range standard deviation σ_r is set to 2 km. To solve the DBT problem in time delay context, the proposed ISE method is combined with IMM-EKF and IMM-PF for comparison. The iteration termination threshold is set to $T/100$. Target typical acceleration used in filter dynamic models is $0.0038\,\mathrm{km/s^2}$, notice that it is mismatched with the second turning. ISE-IMM-PF uses 200 particles for each mode. The Monte Carlo simulation number is 100. However, the number of effective Monte Carlo runs is less than 100, because we consider the runs with a position estimation error at any time index larger than $20\sigma_r$ divergent and cross them out. A record of the number of divergent tracks for different filters is shown in Table 2.

Table 2. Performance comparison of two filters.

	ISE-IMM-EKF	ISE-IMM-PF
Divergent tracks count	16	0
Average RMSE(km)	4.91	1.16
Average computing time(s)	0.0042	2.0148
Average iteration count	4.38	8.45

The root mean square errors (RMSE) of the target position estimated by two filters are shown in Figure 8. ISE-IMM-PF outperforms ISE-IMM-EKF as expected and achieves a RMSE of about 1.3 Km at the end of the observation period, where the distance between observer and target is 27.1 Km.

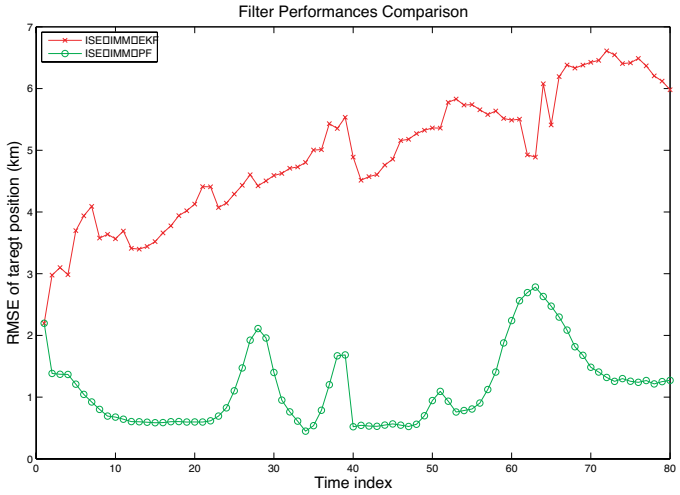

Figure 8. RMSE for tracking scenario illustrated in Figure 8.

For further comparison, Table 2 lists the number of convergent tracks, the values of average RMSE, average computing time per cycle (time step) and average number of iterations per cycle, for both filters.

Note that ISE-IMM-EKF has 16 divergent tracks out of 100 Monte Carlo runs. The other three metrics listed in Table 2 are computed only on convergent tracks. Obviously in such a time-delayed tracking scenario, the overall performance of ISE-IMM-EKF is considered worse than that of ISE-IMM-PF.

A comparison of the average computing time shows that the better performed ISE-IMM-PF suffers from the disadvantage of computational complexity. However, this ISE method tends to be faster than linear search method, since both methods converge to a local optimization solution in less than 10 iterations on average. According to [16], a pair of linear searching bounds in the above scenario can be approximately calculated out to be 3.88 s, 7.02 s. If a step increment is set to 0.05 s (same with the iteration termination threshold), then approximately 63 steps are needed in a searching cycle.

The ISE method behaves well when combined with IMM-PF in the time delay scenario described above. For a detailed comparison see Figure 9: here ISE-IMM-PF takes signal time delay effect into consideration while the conventional IMM-PF does not. The performance improves evidently after ISE method is added.

We can observe that almost the whole RMSE curve of ISE-IMM-PF is below that of IMM-PF. Although ISE-IMM-PF has a larger

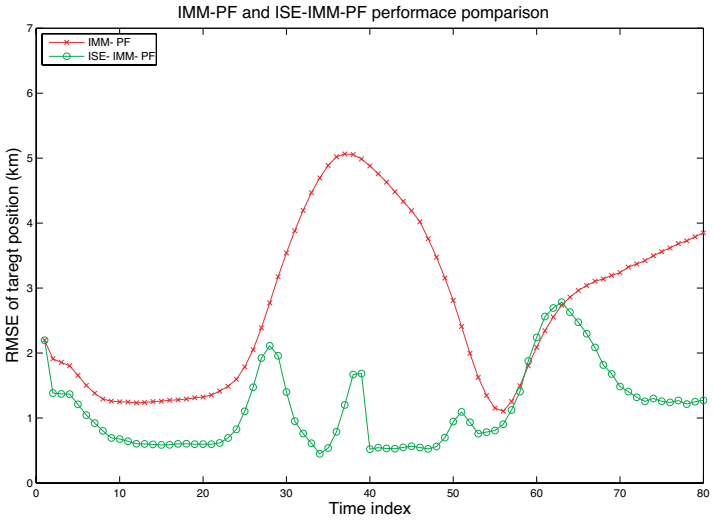

Figure 9. RMSE for ISE-IMM-PF and IMM-PF.

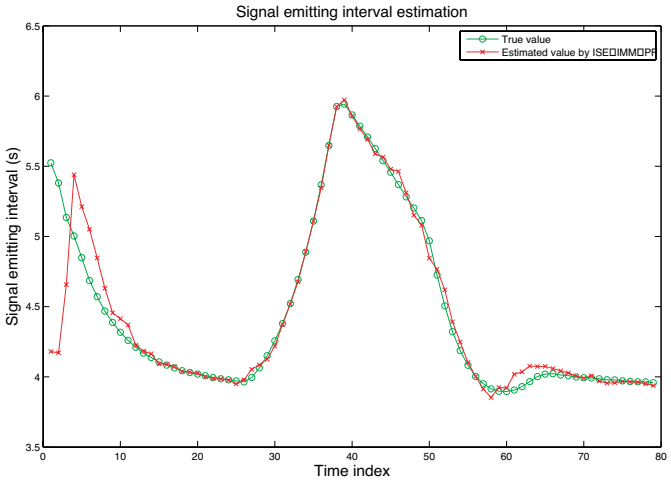

Figure 10. Signal emitting intervals.

RMSE in the second turning stage due to the mode switch error, its RMSE drops to a lower level quickly after the beginning steps of the turning. Since conventional IMM-PF does not have a state prediction stage, it could avoid mode switch error, but time-delayed measurements largely deteriorates its performance.

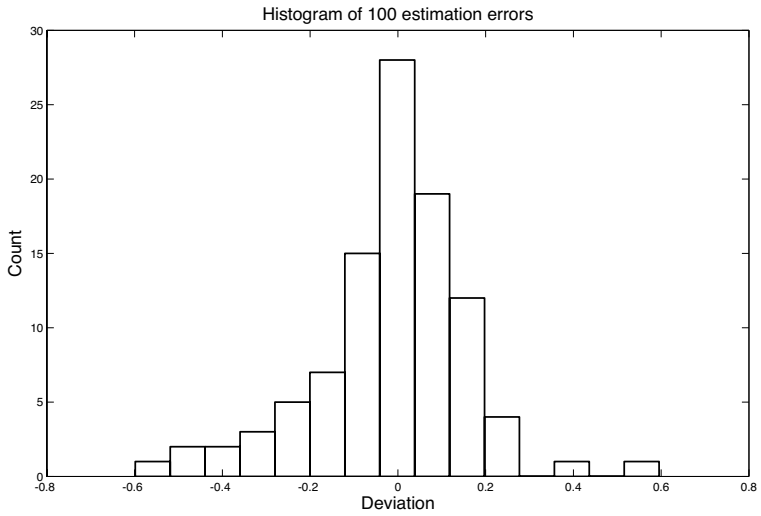

Figure 11. Histogram of 100 estimation errors.

A comparison between the true value of SEI and the estimations by ISE-IMM-PF is illustrated in Figure 10. Though the estimated SEI strongly deviates from the true value in the beginning due to a bad initial density, ISE-IMM-PF manages to decrease the error and obtains a satisfactory estimation after a few steps.

For time step $k = 80$, statistical analysis on 100 estimated values of SEI shows no sign of divergence in this tracking scenario. Figure 11 shows the histogram of 100 estimation errors. All the errors range from $-0.6\,\mathrm{s}$ to $0.6\,\mathrm{s}$, with mean $-0.021\,\mathrm{s}$ and variance $0.0324\,\mathrm{s}^2$.

6. CONCLUSION

In this paper, a general iterative state estimation (ISE) method for time-delayed tracking is described in detail. The method is well suited to IMM maneuvering target estimator and a combination called ISE-IMM is proposed to solve the maneuvering target Doppler-bearing tracking problem in time delay context. Simulations have been carried out to compare the performances of two nonlinear filters in the framework of ISE-IMM in a typical scenario, and the results show the effectiveness and stability of ISE-IMM-PF in combating the negative effect of signal time delay.

REFERENCES

1. Chan, Y. K. and S. Y.Lim, "Synthetic aperture radar (SAR) signal generation," *Progress In Electromagnetics Research B*, Vol. 1, 269–290, 2008.
2. Abdelaziz, A. A., "Improving the performance of an antenna array by using radar absorbing cover," *Progress In Electromagnetics Research Letters*, Vol. 1, 129–138, 2008.
3. Shi, Z. G., S. Qiao, K. S. Chen, W. Z. Cui, W. Ma, T. Jiang, L. X. Ran, "Ambiguity functions of direct chaotic radar employing microwave chaotic Colpitts oscillator," *Progress In Electromagnetics Research*, PIER 77, 1–14, 2007.
4. Garenaux, K., T. Merlet, and M. Alouini, "Recent breakthroughs in RF photonics for radar systems," *IEEE Aerospace and Electronic Systems Magazine*, Vol. 22, No. 2, 3–8, 2007.
5. Wang, C. J., B. Y. Wen, Z. G. Ma, W. D. Yan, and X. J. Huang, "Measurement of river surface current with FWCW radar system," *Journal of Electromagnetic Waves and Applications*, Vol. 21, No. 3, 375–386, 2007.
6. Wang, X., X. Guan, X. Ma, D. Wang, and Y. Su, "Calculating the poles of complex radar targets," *Journal of Electromagnetic Waves and Applications*, Vol. 20, No. 14, 2065–2076, 2006.
7. Singh, A. K., P. Kumar, T. Chakravarty, G. Singh, and S. Bhooshan, "A novel digital beamformer with low angle resolution for vehicle tracking radar," *Progress In Electromagnetics Research*, PIER 66, 229–237, 2006.
8. Turkmen, I. and K. Guney, "Tabu search tracker with adaptive neuro-fuzzy inference system for multiple target tracking," *Progress In Electromagnetics Research*, PIER 65, 169–185, 2006.
9. Stratakos, Y., G. Geroulis, and N. Uzunoglu, "Analysis of glint phenomenon in a monopulse radar in the presence of skin echo and non-ideal interferometer echo signals," *Journal of Electromagnetic Waves and Applications*, Vol. 19, No. 5, 697–711, 2005.
10. Jauffret, C. and Y. Bar-Shalom, "Track formation with bearing and frequency measurements in clutter," *IEEE Transactions on Aerospace and Electronic Systems*, Vol. 26, No. 6, 999–1010, 1990.
11. Ristic, B., S. Arulampalam, and N. Gordon, *Beyond the Kalman Filter: Particle Filters for Tracking Applications*, Artech House, London, 2004.
12. Arulampalam, M. S., B. Ristic, N. Gordon, and T. Mansell, "Bearings-only tracking of manoeuvring targets using particle filters," *EURASIP Journal on Applied Signal Processing*, 2351–

2365, 2004.

13. Ristic, B. and M. S. Arulampalam, "Tracking a manoeuvring target using angle-only measurements: Algorithms and performance," *Signal Processing*, Vol. 83, 1223–1238, 2003.
14. Chan, Y. T. and S. W. Rudnicki, "Bearings-only and Doppler-bearing tracking using instrumental variables," *IEEE Transactions on Aerospace and Electronic Systems*, Vol. 28, No. 4, 1076–1083, 1992.
15. Jauffret, C. and D. Pillon, "Observability in passive target motion analysis," *IEEE Transactions on Aerospace and Electronic Systems*, Vol. 32, No. 4, 1290–1300, 1996.
16. Guo, Y., A. Xue, and D. Peng, "A recursive algorithm for bearings-only tracking with signal time delay," *Signal Processing*, Vol. 88, 1539–1552, 2008.
17. Blom, H. A. P. and Y. Bar-Shalom, "The interacting multiple model algorithm for systems with Markovian switching coefficients," *IEEE Transactions on Automatic Control*, Vol. 33, No. 8, 780–783, 1988.
18. Bar-Shalom, Y., X. R. Li, and T. Kirubarajan, *Estimation with Applications to Tracking and Navigation: Theory Algorithms and Software*, Wiley, New York, 2001.
19. Yang, N., W. Tian, and Z. Jin, "An interacting multiple model particle filter for maneuvering target location," *Meas. Sci. Technol.*, Vol. 17, 1307–1311, 2006.
20. Blom, H. A. P. and E. A. Bloem, "Exact Bayesian and particle filtering of stochastic hybrid system," *IEEE Transactions on Aerospace and Electronic Systems*, Vol. 43, No. 1, 55–70, 2007.
21. Li, X. R. and Y. Bar-Sharlom, "Design of an interacting multiple model algorithm for air traffic control tracking," *IEEE Transactions on Control Systems Technology*, Vol. 1, No. 3, 186–194, 1993.
22. Li, X. R. and V. P. Jilkov, "Survey of maneuvering target tracking Part V: Multiple-model methods," *IEEE Transactions on Aerospace and Electronic Systems*, Vol. 41, No. 4, 1255–1321, 2005.
23. Li, X. R. and Y. Bar-Sharlom, "Multiple-model estimation with variable structure," *IEEE Transactions on Automatic Control*, Vol. 41, No. 4, 1996.
24. Shi, Z. G., S. H. Hong, and K. S. Chen, "Tracking airborne targets hidden in blind Doppler using current statistical model particle filter," *Progress In Electromagenetics Research*, PIER 82, 227–

240, 2008.

25. Arulampalam, M. S., S. Maskell, N. Gordon, and T. Clapp, "A tutorial on particle filters for online nonlinear/non-Gaussian Bayesian tracking," *IEEE Transactions on Signal Processing*, Vol. 50, No. 2, 174–188, 2002.
26. Gordon, N. J., D. J. Salmond, and A. F. M. Smith, "Novel approach to nonlinear/non-Gaussian Bayesian state estimation," *IEE Proceedings-F*, Vol. 140, No. 2, 107–113, 1993.
27. Hong, S. H., Z. G. Shi, and K. S. Chen, "Novel roughening algorithm and hardware architecture for bearings-only tracking using particle filter," *Journal of Electromagnetic Waves and Applications*, Vol. 22, 411–422, 2008.
28. Zang, W., Z. G. Shi, S. C. Du, and K. S. Chen, "Novel roughening method for reentry vehicle tracking using particle filter," *Journal of Electromagnetic Waves and Applications*, Vol. 21, No. 14, 1969–1981, 2007.
29. Gustafsson, F., F. Gunnarsson, N. Bergman, U. Forssell, J. Jansson, R. Karlsson, and R. J. Nordlund, "Particle filters for positioning, navigation, and tracking," *IEEE Transactions on Signal Processing*, Vol. 50, No. 2, 425–437, 2002.
30. Boers, Y. and J. N. Driessen, "Interacting multiple model particle filter," *IEE Proc. — Radar Navig.*, Vol. 150, No. 5, 344–349, 2003.
31. Du, S. C., Z. G. Shi, W. Zang, and K. S. Chen, "Using interacting multiple model particle filter to track airborne targets hidden in blind Doppler," *Journal of Zhejiang University — Science A*, Vol. 8, No. 8, 1277–1282, 2007.
32. Liu, J. S. and R. Chen, "Sequential Monte Carlo methods for dynamic systems," *Journal of the American Statistical Association*, Vol. 93, 1032–1044, 1998.
33. Shensa, M. J., "On uniqueness of Doppler tracking," *J. Acoust. Soc. Am*, Vol. 70, No. 4, 1062–1064, 1981.
34. Passerieux, J. M., D. Pillon, P. Blanc-Benon, and C. Jauffret, "Target motion analysis with bearings and frequencies measurements," *Signals, Systems and Computers, 1988. Twenty-Second Asilomar Conference*, Vol. 1, 458–462, 1988.